

Journal of Materials Chemistry A

Accepted Manuscript



This is an *Accepted Manuscript*, which has been through the Royal Society of Chemistry peer review process and has been accepted for publication.

Accepted Manuscripts are published online shortly after acceptance, before technical editing, formatting and proof reading. Using this free service, authors can make their results available to the community, in citable form, before we publish the edited article. We will replace this *Accepted Manuscript* with the edited and formatted *Advance Article* as soon as it is available.

You can find more information about *Accepted Manuscripts* in the [Information for Authors](#).

Please note that technical editing may introduce minor changes to the text and/or graphics, which may alter content. The journal's standard [Terms & Conditions](#) and the [Ethical guidelines](#) still apply. In no event shall the Royal Society of Chemistry be held responsible for any errors or omissions in this *Accepted Manuscript* or any consequences arising from the use of any information it contains.

Low-cost and Flexible Ultra-thin Silicon Solar Cell Implemented with Energy-down-shift via Cd_{0.5}Zn_{0.5}S/ZnS Core/shell Quantum Dots

Cite this: DOI: 10.1039/x0xx00000x

Received 00th January 2012,
Accepted 00th January 2012

DOI: 10.1039/x0xx00000x

www.rsc.org/

Seung-Wook Baek,^a Jae-Hyoung Shim,^a Yun-Hyuk Ko,^a Jin-Seong Park,^a Gon-Sub Lee,^a Mohammed Jalalah,^{a,b} M. S. Al-Assiri,^b and Jea-Gun Park,^{a*}

Flexible ultra-thin silicon (~30- μ m thickness) solar cells implemented with an energy-down-shift layer showed stable flexible and twistable characteristics. In particular, spin-coating Cd_{0.5}Zn_{0.5}S/ZnS core/shell quantum dots (QDs) on the cells enhanced the PCE by ~0.7 % through an energy-down-shift effect that enhanced the external quantum efficiency at the UV light region. In addition, the cells demonstrated excellent bending fatigue performance since their PCE levels were sustained at ~12.4 % after 5000 bending cycles under ~5.72 % strain.

Introduction

For the past few decades, flexible or bendable silicon^{1,2}, dye-sensitized^{3,4}, organic⁵⁻⁷, and hybrid solar cells^{8,9} have been intensively researched as means to improve power conversion efficiency (PCE) and minimize cell fabrication cost because of their attractive applications, which include building-integrated photovoltaic (BIPV), electronics-integrated photovoltaic (EIPV), portable electronics power, and automobile-integrated photovoltaic applications. Although flexible or bendable dye-sensitized, organic, and hybrid solar cells have demonstrated reasonable PCE and fabrication cost for actual photovoltaic application, their PCE value are still quite lower and their fabrication costs higher than those of solid silicon solar cells. Recently, S. Jeong et al.¹⁰ reported ultra-thin silicon (~10- μ m thickness) solar cell showing a maximum PCE of 13.7 %. However, it was fabricated with typical high-cost semiconductor device processes such as SOI wafer, photolithography, and deep reactive-ion etching. In addition, it could not demonstrate good flexible or bendable characteristics. Thus, we developed a flexible ultra-thin silicon solar cell implemented with an energy-down-shift layer comprising Cd_{0.5}Zn_{0.5}S/ZnS core/shell quantum dots (QDs)¹¹⁻¹³. Of particular note is that, to fabricate solar cells at low cost, we introduced ultra-thin silicon (~30- μ m thickness) via Potassium hydroxide (KOH) etching, p-n junction formation via phosphoryl chloride (POCl₃) doping, back surface field formation via thin aluminium (Al) film evaporation and rapid thermal annealing, top electrode patterning via thin film silver (Ag) evaporation, anti-reflective coating via a silicon nitride (SiN_x) anti-reflective film formed by plasma-enhanced chemical vapor deposition, and core/shell QD spin-coating. In addition, to enhance PCE at the ultraviolet (UV) wavelength region, we implemented an energy-down-shift layer by coating Cd_{0.5}Zn_{0.5}S/ZnS core/shell QDs on flexible ultra-thin silicon solar cells. In our study, we characterized physical, optical,

electrical, and flexible properties in detail to achieve flexible ultra-thin silicon solar cells implemented with an energy-down-shift layer.

Results and discussion

The detailed vertical structure of our developed flexible ultra-thin silicon solar cell implemented with an energy-down-shift layer comprises a ~10-nm thick energy-down-shift layer spin-coated with Cd_{0.5}Zn_{0.5}S/ZnS core/shell QDs, a ~95-nm thick SiN_x anti-reflective film, a ~500-nm thick Ag front-side electrode, a ~30- μ m thick silicon including a p/n junction, a ~700-nm Al back-side electrode, and a ~180- μ m thick flexible polyethylene terephthalate (PET) substrate, as shown in Fig. 1a. The cell exhibited good flexible and twistable characteristics, which are useful for installing solar cells on curved surfaces of buildings or automobiles (Fig. 1b) and on wearable devices (Fig. 1c and Video 1). In addition, a flexible ultra-thin silicon solar cell implemented with an energy-down-shift layer did not emit any light after exposing visible light on the solar cell surface while it emitted visible light after exposing UV light on the solar-cell surface, as shown in Fig. 1d. Furthermore, it demonstrated good fatigue performance, as shown in Fig. 1e, which we will be show by citing statistical data.

The physical, chemical, and optical properties of the Cd_{0.5}Zn_{0.5}S/ZnS core/shell QDs demonstrated energy-down-shift, as shown in Fig. 2. The QDs showed a spherical shape, were well crystallized, and were well dispersed with each other, as shown in Fig. 2a. The average QD diameter was ~6.7 nm, as shown in Fig. 2b. Figure 2c shows an energy dispersion X-ray spectroscopy (EDX) line scan and a transmission electron microscope (TEM) image, which evidently depict a core/shell QD structure in which the chemical composition of the ~4.0-nm diameter core QDs was Cd_{0.5}Zn_{0.5}S while that of the 1.3-nm diameter shell QDs was ZnS. Note that the core QDs'

$\text{Cd}_{0.5}\text{Zn}_{0.5}\text{S}$ composition was confirmed through exact recalculation performed by considering the volume of the core QDs, although the EDX line scan indicated $\text{Cd}_{0.19}\text{Zn}_{0.43}\text{S}_{0.38}$ composition. Figure 2d shows the crystalline structure of the $\text{Cd}_{0.5}\text{Zn}_{0.5}\text{S}/\text{ZnS}$ core/shell QDs, which was characterized by X-ray diffraction (XRD). The $\text{Cd}_{0.5}\text{Zn}_{0.5}\text{S}$ core QDs peaked at (100), (002), (110), and (112) which were observed at 26.44° , 28.22° , 46.66° , and 55.43° while the ZnS shell QDs peaked at (111), (220), and (311), which were observed at 28.26° , 46.99° , and 55.74° , respectively (JCPDS Cards: 01-9251, 12-6328). The XRD results indicate that the crystalline structure of the core QDs was hexagonal while that of the shell QDs was a wurtzite structure. In addition, Scherrer's equation of XRD patterns showed the core QDs were 3.9 nm in diameter, which was similar to the diameter observed by TEM-EDX. The diameter using Scherrer's equation (1) is given by¹⁴

$$\tau = \frac{K\lambda}{\beta \cos\theta} \quad (1)$$

where τ is the mean size of the crystalline domains, K is a dimensionless shape factor, β is the line broadening at half the maximum intensity (FWHM), and θ is the Bragg angle. To confirm the energy-down-shift of the core/shell QDs, UV visible spectroscopy and photo-luminescence (PL) were used to measure the absorption of UV followed by the emission of visible light, which is the concept of energy-down-shift, as shown in Fig. 2e. In a quartz cuvette, a 0.3-wt% $\text{Cd}_{0.5}\text{Zn}_{0.5}\text{S}/\text{ZnS}$ core/shell QDs solution absorbed $\sim 100\%$ light in the wavelength between 250 and 450 nm (the red solid line in Fig. 2e) and emitted blue light (442 nm) after UV light was exposed through the cuvette (the left image in Fig. 2e inset). In addition, a thin film layer on glass spin-coated with the 0.3-wt% core/shell QDs solution absorbed $\sim 80\%$ light in the wavelength between 220 and 450 nm (the green solid line in Fig. 2e). A thin film layer on a flexible ultra-thin silicon solar cell spin-coated with the 0.3-wt% core/shell QDs solution emitted blue light after being exposed to UV light (the right image in Fig. 2e inset). Furthermore, the 0.3-wt% core/shell QDs solution in the cuvette emitted a 442-nm wavelength PL signal with 79.9 % the quantum yield using Rhodamine 6G in ethanol as a reference¹⁵ (80.2% using Quinine sulfate in 0.5M H_2SO_4 as a reference)¹⁶, as shown in the blue solid line of Fig. 2e. The optical properties in Fig. 2e evidently demonstrated energy-down-shift in which the core/shell QDs absorbed UV light in wavelengths between 250 and 450 nm and emitted 442-nm wavelength blue light. The emitted 442-nm wavelength blue light would be produced via the exciton recombination process at the $\text{Cd}_{0.5}\text{Zn}_{0.5}\text{S}$ core quantum-dot and the red shift induced by the compressive strain at the interface between the $\text{Cd}_{0.5}\text{Zn}_{0.5}\text{S}$ core QD and ZnS shell QD (see Supplementary Table 1). Note that the wavelength and quantum yield of the emitted blue light from the $\text{Cd}_{1-x}\text{Zn}_x\text{S}/\text{ZnS}$ core/shell QDs strongly depended on the ZnS shell thickness (see Supplementary Fig. 1).^{17, 18} In addition, the core/shell QDs's optical properties showed the energy band gap of the core QDs was ~ 2.81 eV¹⁹, corresponding to the emitted 442-nm wavelength PL signal (blue visible light) while that of the shell QDs was ~ 3.56 eV²⁰, corresponding to the absorption of ~ 301 -nm wavelength UV light, as shown in Fig. 3f. Since the energy band gap of the shell QDs (~ 3.56 eV) was higher than that of the core QDs (~ 2.81 eV), and since the diameter of the core QDs (~ 4.0 nm) is considerably small, the core QDs would be easily quantized with E1, E2, E3 etc. and H1, H2, H3 etc., where E and H are

the quantized states for the electrons and the holes and the subscript is the quantum number. Thus, the core/shell QDs would absorb UV light in wavelengths between 250 and 450 nm and then generate electron-hole pairs at E2 and H1 or E3 and H1. Afterward, the excited electrons would be transitioned from E3 to E1 or from E2 to E1 by transferring thermal energy to the $\text{Cd}_{0.5}\text{Zn}_{0.5}\text{S}$ core QD lattices. Finally, the recombination of electrons at E1 and holes at H1 would emit 442-nm wavelength blue light, performing energy-down-shift. Therefore, implementing the $\text{Cd}_{0.5}\text{Zn}_{0.5}\text{S}/\text{ZnS}$ core/shell QDs via spin-coating them on the surface of a flexible ultra-thin silicon solar cell would absorb UV light and then emit blue light. The emitted blue light would be reabsorbed through the cell's surface, resulting in enhanced external quantum efficiency (EQE) at the UV light wavelength region. Note that a silicon solar cell could not absorb the UV light because of the ~ 1.1 eV energy band gap of Si.

To confirm the optical properties of the flexible ultra-thin silicon solar cell implemented with the $\text{Cd}_{0.5}\text{Zn}_{0.5}\text{S}/\text{ZnS}$ core/shell QDs, the cross-sectional surface structure was observed by TEM and the surface reflectance was measured as a function of wavelength. The core/shell QDs were coated on a 95-nm thick SiN_x anti-reflective film surface within one layer and well dispersed to one another, as shown in Fig. 3a. The surface reflectance of an ultra-thin silicon solar cell without the anti-reflective film and QD layer rapidly decreased from ~ 69 to 32 % when the wavelength was increased from 250 to 1100, as shown in Fig. 3b. Furthermore, the depositing the anti-reflective film on the cell sharply reduced the surface reflectance because of the anti-reflective layer's effects, i.e., the surface reflectance peaked at $\sim 47\%$ at ~ 400 -nm wavelength and dropped to $\sim 7\%$ at wavelengths between 700 and 1000 nm. In addition, spin-coating the core/shell QDs on the anti-reflective film showed a dependency of surface reflectance on wavelength similar to that obtained by merely depositing the anti-reflective film on the cell. However, spin-coating the core/shell QDs reduced the surface reflectance to $\sim 10\%$ at the peak wavelength (~ 400 nm), demonstrating evidence of energy-down-shift.

To investigate the photovoltaic performance for the cell implemented with the core/shell QDs layer, EQE was estimated as a function of wavelength. The EQE for a cell without the anti-reflective film and without the QDs layer increased from ~ 23 to $\sim 62\%$ when the wavelength increased from 300 to ~ 600 nm and then decreased from ~ 62 to less than 6 % when the wavelength decreased from 600 to 1100 nm. It peaked at $\sim 62\%$ at 600-nm wavelength, as shown in Fig. 4a. Furthermore, depositing the anti-reflective film on the cell slightly increased EQE by $\sim 10\%$ at the UV light region (300-400 nm) while it greatly increased it by $\sim 24\%$ at the visible light region (400-950 nm). Note that the EQE strongly depended on the anti-reflective film thickness (see Supplementary Fig. 2). In particular, spin-coating the core/shell QDs on the anti-reflective film considerably increased the EQE by $\sim 27\%$ at the UV light region, but did not enhance it at the visible light region (400-900 nm), thus demonstrating energy-down-shift. These results indicate that depositing the anti-reflective film mainly enhances the EQE at the visible light region (400-950 nm) while spin-coating the core/shell QDs principally enhances it at the UV light region (300-400 nm). In addition, the surface reflectance in Fig. 2b is well correlated with the EQE in Fig. 3b: i.e., a lower surface reflectance leads to a high EQE.

The effects of the anti-reflective film and the core/shell QDs layer on the electrical performances of the flexible ultra-thin

silicon solar cells are shown in Fig. 4b (Supplementary Fig. 3). The short-circuit current density (J_{SC}), open circuit voltage (V_{OC}), fill factor (FF), and PCE for an ultra-thin silicon solar cell without the anti-reflective film and the QDs layer were 21.52 mA/cm², 0.495 V, 75.74 %, and 8.07 %, respectively. For a cell with the anti-reflective film, the J_{SC} sharply increased from 21.52 to 31.35 mA/cm² while the V_{OC} and FF did not change, resulting in the PCE being substantially enhanced from 8.07 to 11.70 %. In addition, with the core/shell QDs on the anti-reflective film, the J_{SC} considerably increased from 31.35 to 33.05 mA/cm² because of the energy-down-shift effect while the V_{OC} and FF did not change, thereby increasing the PCE from 11.70 to 12.37 %, as can be seen by comparing Fig. 4a with Fig. 4b. These results imply that depositing the anti-reflective film enhances the J_{SC} mainly due to the anti-reflective layer effect, while spin-coating the core/shell QDs mainly enhances it because of the energy-down-shift effect. In particular, comparing Fig. 4a with Fig. 4b demonstrates the energy-down-shift effect that the core/shell QDs absorb the UV light and emit visible light (blue light) and the emitted visible light is reabsorbed into the cell.

To evaluate the bending fatigue characteristic for the cell implemented with the core/shell QDs, a bending test was performed under the conditions of a 12.7-mm bending radius (r) and a 5,000 bending cycles, as shown in Fig. 5. The applied strain for this bending test was ~5.72 %, as calculated by equation (2).²¹

$$\epsilon = \left(\frac{d_f + d_s}{2R} \right) \cdot \frac{(1 + 2\eta + \chi\eta^2)}{(1 + \eta)(1 + \chi\eta)} \quad (2)$$

where, ϵ is the strain, R is the bending radius, χ is Y_f/Y_s , Y_f , Y_s are the Young's moduli of the film and substrate, η is d_f/d_s , d_f , d_s are the film and substrate thickness. The flexible characteristic for a cell implemented with the core/shell QDs was well demonstrated in Video 2. In particular, when exposed to UV light, the cell emitted blue light under the bending test, as shown in Fig. 5a and Video 3, 4. All the cells showed a good bending fatigue characteristic, i.e., their PCE values did not change after 5,000 bending cycles, as shown in Fig. 5b. The dependencies of J_{SC} and V_{OC} on the bending cycles are shown in Supplementary Fig. 4. Thus, the cells implemented with the core/shell QDs achieved good bending fatigue results with a high PCE (~12.37 %).

Experimental

Quantum dot synthesis

A hot injection method synthesized the Cd_{0.5}Zn_{0.5}S/ZnS core/shell QDs. In the synthesis process, 1 mmol of cadmium oxide (CdO), 7.5 mL of oleic acid (OA), and 10 mmol of zinc oxide (ZnO) were mixed at room temperature and reacted at 150 °C. After reaching 150 °C, the reaction flask was filled with N₂ gas and injected with 15 mL of 1-octadecene (1-ODE). Subsequently, the distilled mixture was heated up to 300 °C to produce a transparent solution of Cd(OA)₂ and Zn(OA)₂. Then 2 mmol of sulfur powder was dissolved in 3 mL of 1-ODE and purge with N₂, and the purged sulfur solution was quickly injected into the reaction flask and reacted. After the sulfur precursor was injected, the temperature of the reaction flask was elevated to 310 °C for growing the Cd_{0.5}Zn_{0.5}S core QDs (nucleation process). After 8 min had elapsed, the N₂ purged sulfur solution was introduced into the reactor to cap the

existing Cd_{0.5}Zn_{0.5}S core QDs with the ZnS shell without any purification step at the time when 8 mmol of sulfur powder was dissolved in 5mL of OA. After allowing 40 min to elapse to produce the ZnS shell, the solution dispersed with QDs was cooled down at room temperature and then centrifuged with an additional amount of methanol and acetone to eliminate impurities. Finally, the precipitated QDs were re-dispersed with chloroform. The detailed morphology, size distribution, absorption, chemical composition ratio, and PL for the QDs were characterized by high-resolution TEM at 200 kV, UV visible spectroscopy, XRD, EDX line-scan profile and PL spectroscopy using a HeCd laser source with 325-nm wavelength. The quantum yield (QY) of the QDs was measured and estimated by comparing their fluorescence intensities with those of primary standard solutions (QY: 95 % Rhodamine 6G in ethanol and 54 % quinine sulfate in 0.5M H₂SO₄) at the same optical density (optical density=0.05) and excitation wavelength (325 nm).

Solar-cell fabrication

Figure 6 shows the fabrication flow of the flexible ultra-thin silicon solar cells implemented with an energy-down-shift layer. Single-crystal silicon wafers doped with boron (10 Ωcm) were used and cut into 50×50 mm² areas and 725 μm thick. The wafers were etched using KOH at 90 °C for 8.5 h, reducing the thickness to ~30 μm, producing a flexible ultra-thin silicon substrate. When attached to Ethylene-vinyl acetate (EVA) and PET films, the substrate showed flexible or twistable characteristics, as demonstrated in Video 5 and 6. Since the EVA film showed a weak thermal characteristic, the PET film was selected as a holding substrate for the flexible ultra-thin silicon substrate. To fabricate solar cells, the silicon substrate samples were submitted to POCl₃ diffusion at 790 °C for 15 min and drive-in at 810 °C for 5 min to produce an n-doping layer, resulting in 125 Ω/□ emitter resistance. Afterward, the silicon substrates were etched by using diluted hydrofluoric acid to remove the phosphorous silicate glass film. Bottom Al electrodes 700-nm thick were thermally evaporated at 3.0 Å/s evaporation rate. To form the back surface field, they were heat-treated using rapid thermal annealing at 400 °C for 1 s. Top Ag electrodes 500-nm thick were thermally evaporated at a 2.0 Å/s evaporation rate. Then, a 95-nm thick SiN_x anti-reflective film was deposited by low frequency plasma enhanced chemical vapour deposition. Note that the anti-reflective film showed a maximum EQE (see Supplementary Fig. 2). A 0.3-wt% Cd_{0.5}Zn_{0.5}S/ZnS core/shell QDs solution was dropped on the cell coated with the anti-reflective film, then the cell was spin-coated at 1,000 rpm for 60 s and annealed at 95 °C for 10 min to dry the solvent of the QDs solution. The thickness of the ~0.3-wt% QDs layer after spin-coating was ~7.9-nm, as measured by TEM. The surface reflectance of the flexible ultra-thin silicon solar-cells was estimated by using UV-visible light spectrometry (Varian Cary-5000 UV-Visible Spectrophotometer). Photovoltaic performances such as J_{SC} , V_{OC} , FF, and PCE were estimated by using a solar simulator (McScience LAB-160).

Conclusions

A flexible ultra-thin silicon (~30-μm thickness) solar cell substrate was produced by a simple low-cost wet etching process using KOH and demonstrated excellent twistable or flexible characteristics. New low-cost solar cell fabrication processes were used to produce a flexible ultra-thin silicon

solar-cell substrate, e.g., thermal Al evaporation followed by rapid thermal annealing at 400 °C for 1 sec for the back-side electrode, thermal Ag evaporation without firing for the front-side electrode, and SiN_x anti-reflective layer deposition after the front-side electrode formation. In addition, the implementing an energy-down-shift layer via spin-coating Cd_{0.5}Zn_{0.5}S/ZnS core/shell QDs on the cell increased PCE to 12.4 % since the core/shell QDs absorb UV light and emit visible light (blue light), and the emitted visible light reabsorbs into the cell. In particular, the fabrication cost and PCE (12.4 %) for cells implemented with the energy-down-shift layer would be cheaper and higher than those for previous flexible silicon-based solar cells (i.e., silicon nanowire²², silicon pyramid²³, silicon nanocone²⁴ hybrid organic-inorganic silicon solar cell). Note that flexible dye-sensitized solar cells³, flexible hybrid organic-inorganic solar cells⁹, and flexible organic solar cells⁶ have achieved PCE of ~5.8, 12, and 8.4 %, respectively. Furthermore, our developed solar cells implemented with an energy-down-shift layer demonstrated an excellent bending-fatigue performance for up to 5,000 bending cycles with 5.72 % strain. This makes them practical and suitable, for BIPV, EIPV, portable electronics power, and automobile-integrated photovoltaic applications. Implementing the ultra-thin cells with an energy-down-shift layer comprising core/shell QDs and with energy-up-conversion via doped core/shell QDs could further enhance the PCE of flexible silicon solar cells. Note that the doped core/shell QDs providing energy-up-conversion absorb infra-red light and then emit visible light that is reabsorbed into the cell. Thus, further study on flexible ultra-thin silicon solar cells implemented with energy-up-conversion will be necessary to maximize the PCE of the cells^{25, 26}.

Acknowledgements

This work was supported by the Brain Korea 21 PLUS Program in 2014 and the Ministry of Higher Education, Kingdom of Saudi Arabia for supporting this research through a grant (PCSED-008-14) under the Promising Centre for Sensors and Electronic Devices (PCSED) at Najran University, Kingdom of Saudi Arabia.

Notes and references

^a Department of Electronics, Hanyang University, Seoul 133–791, Republic of Korea. Fax: +82 2 2220 1179; Tel:+82 2 2220 0234; E-mail: parkjg@hanyang.ac.kr

^b Promising Center for Sensors and Electronic Devices (PCSED), Najran University, P.O. Box 1988, Najran 11001, Saudi Arabia.

† Footnotes should appear here. These might include comments relevant to but not central to the matter under discussion, limited experimental and spectral data, and crystallographic data.

Electronic Supplementary Information (ESI) available: [details of any supplementary information available should be included here]. See DOI: 10.1039/b000000x/

1. D. H. Lee, J. Y. Kwon, S. Maldonado, A. Tuteja and A. Boukai, *Nano letters*, 2014, 14, 1961-1967.
2. S. Wang, B. D. Weil, Y. Li, K. X. Wang, E. Garnett, S. Fan and Y. Cui, *Nano letters*, 2013, 13, 4393-4398.
3. M. J. Yun, S. I. Cha, S. H. Seo and D. Y. Lee, *Sci. Rep.*, 2014, 4, 5322.
4. J. Zhang, M. He, N. Fu, J. Li and X. Yin, *Nanoscale*, 2014, 6, 4211-4216.

5. W. Wang, T.-S. Bae, Y. H. Park, D. H. Kim, S. Lee, G. Min, G.-H. Lee, M. Song and J. Yun, *Nanoscale*, 2014, 6, 6911-6924.
6. K.-S. Chen, H.-L. Yip, J.-F. Salinas, Y.-X. Xu, C.-C. Chueh and A. K. Y. Jen, *Advanced Materials*, 2014, 26, 3349-3354.
7. C. J. An, C. Cho, J. K. Choi, J.-M. Park, M. L. Jin, J.-Y. Lee and H.-T. Jung, *Small*, 2014, 10, 1278-1283.
8. C. Fradler, T. Rath, S. Dunst, I. Letofsky-Papst, R. Saf, B. Kunert, F. Hofer, R. Resel and G. Trimmel, *Solar Energy Materials and Solar Cells*, 2014, 124, 117-125.
9. S. Thiyagu, C.-C. Hsueh, C.-T. Liu, H.-J. Syu, T.-C. Lin and C.-F. Lin, *Nanoscale*, 2014, 6, 3361-3366.
10. S. Jeong, M. D. McGehee and Y. Cui, *Nat Commun*, 2013, 4, 2950.
11. S.-W. Baek, J.-H. Shim, H.-M. Seung, G.-S. Lee, J.-P. Hong, K.-S. Lee and J.-G. Park, *Nanoscale*, 2014, 6, 12524-12531.
12. S.-W. Baek, J.-H. Shim and J.-G. Park, *Physical Chemistry Chemical Physics*, 2014, 16, 18205-18210.
13. X. Huang, S. Han, W. Huang and X. Liu, *Chemical Society reviews*, 2013, 42, 173-201.
14. C. Koch, I. Ovid'ko, S. Seal and S. Veprek, *Structural Nanocrystalline Materials: Fundamentals and Applications*, Cambridge University Press, 2007.
15. M. Fischer and J. Georges, *Chemical Physics Letters*, 1996, 260, 115-118.
16. A. N. Fletcher, *Photochemistry and Photobiology*, 1969, 9, 439-444.
17. W. K. Bae, M. K. Nam, K. Char and S. Lee, *Chemistry of Materials*, 2008, 20, 5307-5313.
18. K.-H. Lee, J.-H. Lee, W.-S. Song, H. Ko, C. Lee, J.-H. Lee and H. Yang, *ACS Nano*, 2013, 7, 7295-7302.
19. J. J. Sharkey, A. J. Peter and L. Chang Woo, *Quantum Electronics, IEEE Journal of*, 2011, 47, 1451-1457.
20. O. E. Jaime-Acuña, H. Villavicencio, J. A. Díaz-Hernández, V. Petranovskii, M. Herrera and O. Raymond-Herrera, *Chemistry of Materials*, 2014, DOI: 10.1021/cm5024585.
21. G. Crawford, *Flexible Flat Panel Displays*, Wiley, 2005.
22. H.-J. Syu, S.-C. Shiu, Y. Hung, Jr., C.-C. Hsueh, T.-C. Lin, T. Subramani, S.-L. Lee and C.-F. Lin, *Progress in Photovoltaics: Research and Applications*, 2013, 21, 1400-1410.
23. T.-G. Chen, B.-Y. Huang, E.-C. Chen, P. Yu and H.-F. Meng, *Applied Physics Letters*, 2012, 101, 033301.
24. S. Jeong, E. C. Garnett, S. Wang, Z. Yu, S. Fan, M. L. Brongersma, M. D. McGehee and Y. Cui, *Nano letters*, 2012, 12, 2971-2976.
25. M. T. Nimmo, L. M. Caillard, W. De Benedetti, H. M. Nguyen, O. Seitz, Y. N. Gartstein, Y. J. Chabal and A. V. Malko, *ACS Nano*, 2013, 7, 3236-3245.
26. W. Yan, J. Lei, Z. Bingbo, Y. Peihao, Q. Yanyan, S. Daqian, Z. Juying and L. Qi, *Nanotechnology*, 2013, 24, 175101.

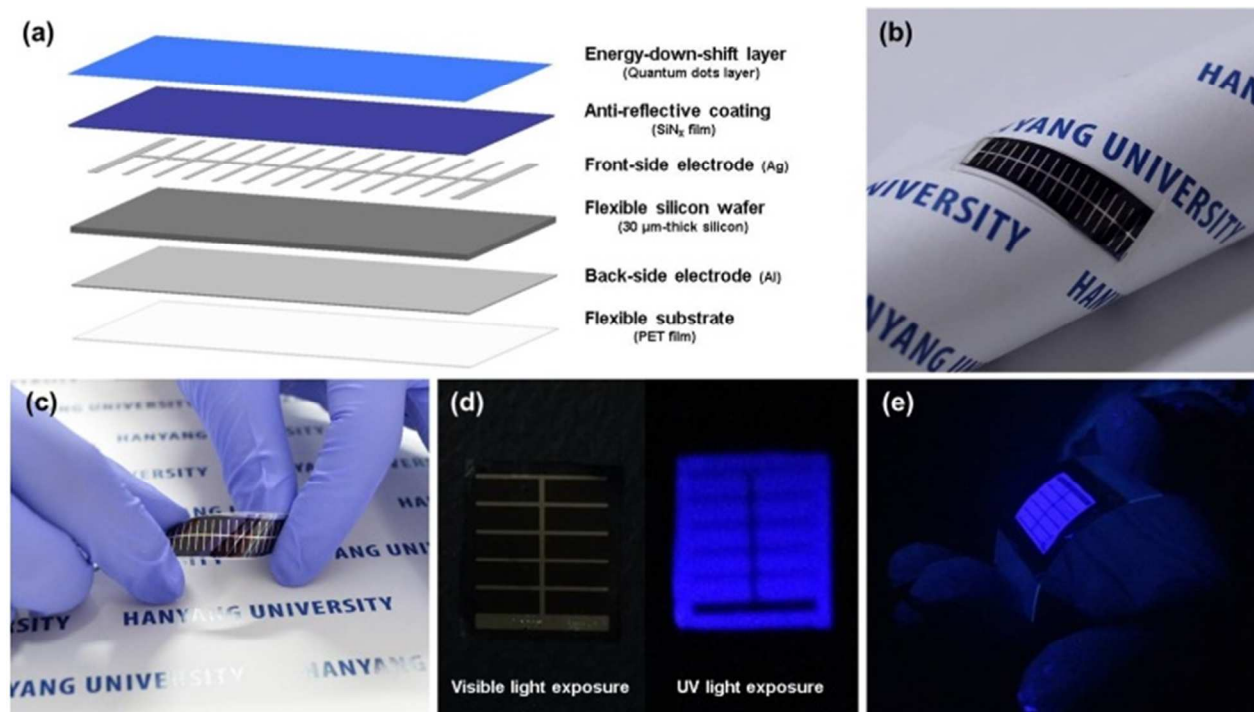


Figure 1 Physical and optical properties of flexible ultra-thin silicon solar-cells implemented with energy-down-shift layer. (a) Vertical structure schematic. (b) Photo showing bendability. (c) Photo showing twistability (Video 1). (d) Photo showing energy-down-shift. (e) Photo showing flexibility.

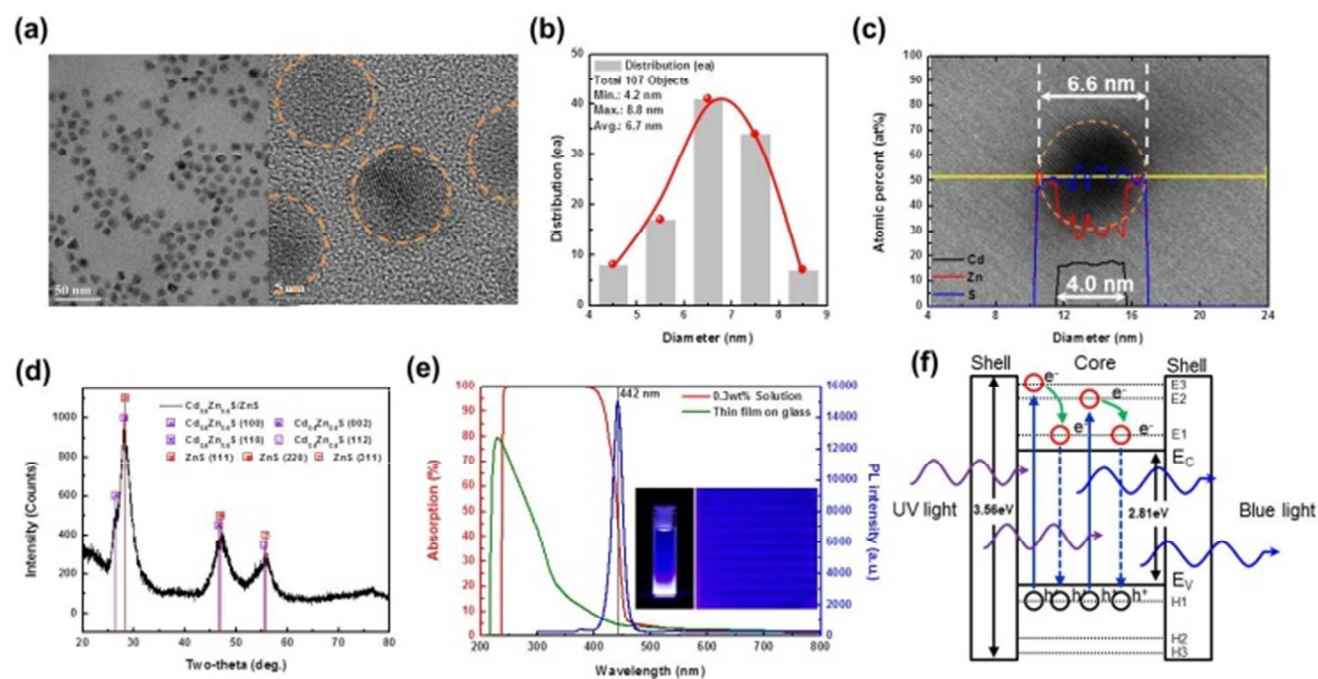


Figure 2 Physical, chemical, and optical properties of $\text{Cd}_{0.5}\text{Zn}_{0.5}\text{S}/\text{ZnS}$ core/shell QDs. (a) Top-view HR-TEM images. (b) Size distribution. (c) Chemical composition profile by TEM line-profile. (d) Crystalline characteristics by XRD. (e) Photo showing absorption, photo-luminescence, and light emission. (f) Modeled energy band diagram.

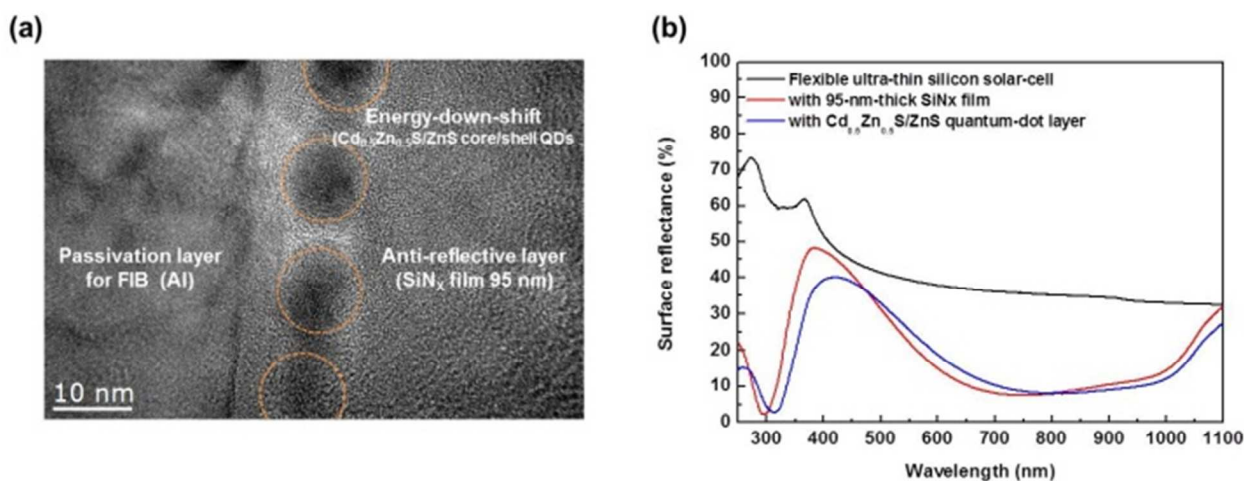


Figure 3 Photovoltaic performance of flexible ultra-thin silicon solar-cell implemented with energy-down-shift layer. (a) Cross-sectional structure of $\text{Cd}_{0.5}\text{Zn}_{0.5}\text{S}/\text{ZnS}$ core/shell QDs layer spin-coated on 95-nm thick SiN_x anti-reflective film. (b) Surface reflectance as a function of wavelength.

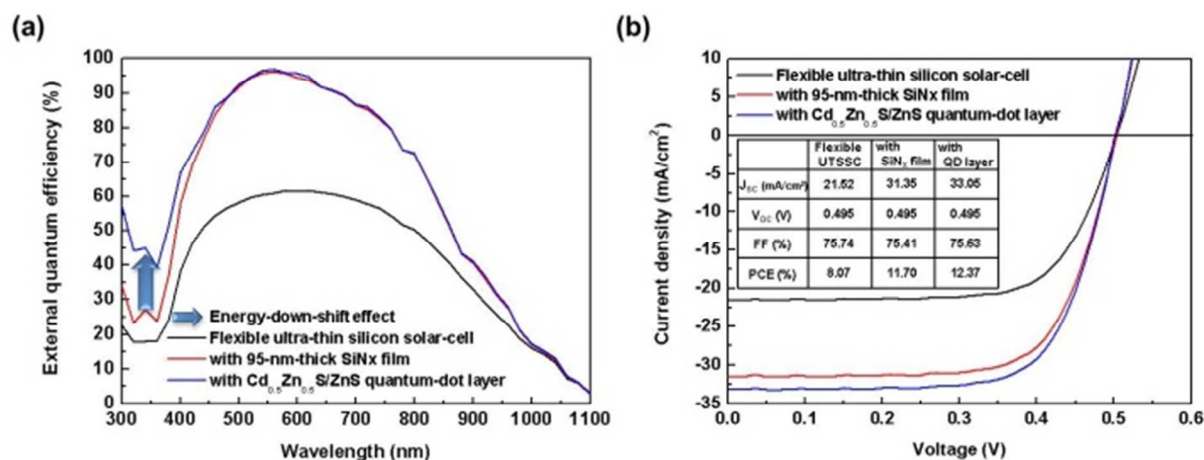


Figure 4 Physical Electrical performance of flexible ultra-thin silicon solar-cell implemented with energy-down-shift layer. (a) EQE as a function of wave length. (b) Current density (J) vs. voltage (V) curve, J_{SC} , V_{OC} , FF, and PCE.

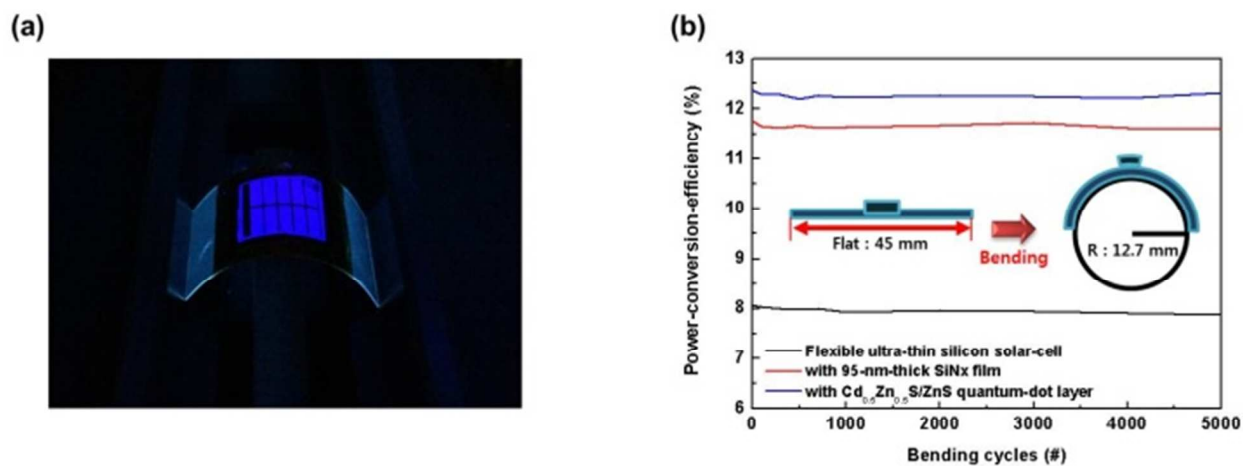


Figure 5 Physical Bending fatigue performance of flexible ultra-thin silicon solar cell implemented with energy-down-shift layer. (a) Photo showing bendability under $\sim 5.72\%$ strain (Video 2, 3). (b) PEC as a function of number of bending cycles.

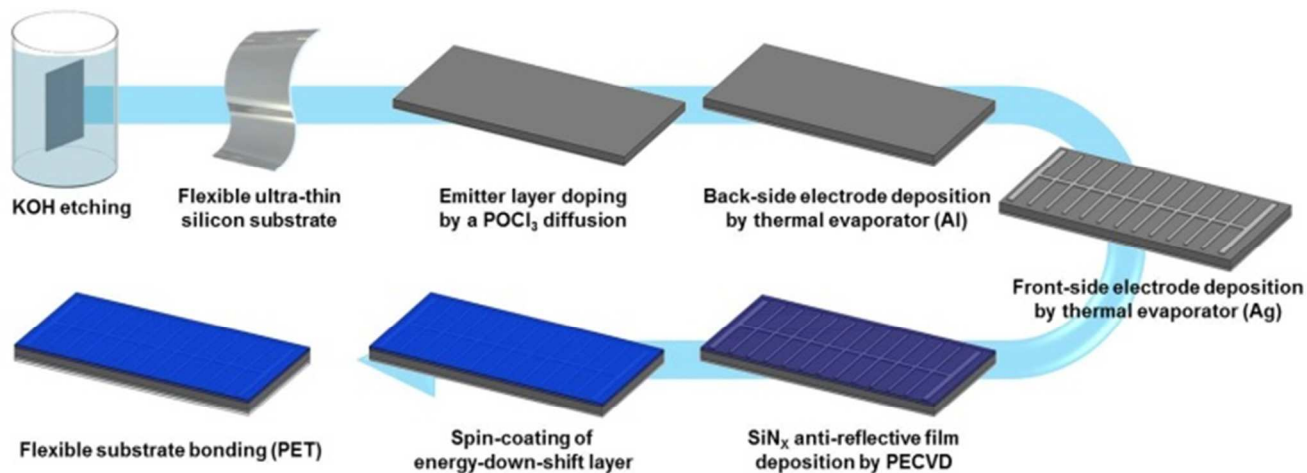


Figure 6 Fabrication flow of flexible ultra-thin silicon solar-cell implemented with energy-down-shift layer.